Hindawi Publishing Corporation
Journal of Control Science and Engineering
Volume 2007, Article ID 36319, 10 pages
doi:10.1155/2007/36319

Research Article

Detection of Surface Defects on Compact Discs

P. F. Odgaard,[1,2] J. Stoustrup,[2] and P. Andersen[2]

[1] *KK-Electronic a/s, Jens Juuls Vej 40, 8260 Viby J, Denmark*
[2] *Section of Automation and Control, Department of Electronic Systems, Aalborg University, Fredrik Bajers Vej 7C, 9220 Aalborg, Denmark*

Received 15 November 2006; Revised 23 April 2007; Accepted 13 August 2007

Recommended by Tomas McKelvey

Online detection of surface defects on optical discs is of high importance for the accommodation schemes handling these defects. These surface defects introduce defect components to the position measurements of focus and radial tracking positions. The respective controllers will accordingly try to suppress these defect components resulting in a wrong positioning of the optical disc drive. In this paper, two novel schemes for detecting these surface defects are introduced and compared. Both methods, which are an extended threshold scheme and a wavelet packet-based scheme, improve the detection compared with a standard threshold scheme. The extended threshold scheme detects the four tested defects with a maximal detection delay of 3 samples while the wavelet packet-based scheme has a maximal detection delay of 6 samples. Simulations of focus and radial positions in the presence of a surface defect are performed in order to inspect the importance and consequences of the size of the detection delay, from which it can be seen that focus and radial position errors increase significantly due to the defect as the detection delay increases.

1. INTRODUCTION

Although CD and DVD disc drives are mature technologies, playing discs with severe surface-defects still cause problems for typical disc drives. The user most often inflicts these surface-defects on the disc during handling. Touching or placement on unclean surfaces can cause scratches, fingerprints, and dust on the disc surface. The problem with these surface-defects is that they dramatically lower the quality of the optical detector signals used for positioning of the optical pick-up, reading the information on the disc. Based on these optical position measurements, two control loops are formed to position the optical pick-up in focus and radial directions.

A large amount of research is done in the field of nominal control of these positioning loops. Examples of different applied methodologies follow subsequently. The first application of a μ-controller used in a CD player was reported in [1], which was based on DK iterations. An example of an adaptive control design was [2], where a self-tuning controller was suggested. Automatic adjustment of gains in dependence of the reflective characteristics is standard in commercial CD players. An adaptive repetitive method was suggested in [3], a quantitative feedback theory was used in [4]. In [5], a hybrid fuzzy control was designed. [6] improves on the repetitive control scheme for a reaction to the repetitive reference.

Some work has already been done for handling these surface-defects, see [7–10]. All these methods are based on a defect tolerant controller strategy in which the surface-defects are detected and subsequently handled in some manor. Some related work on classification of surface-defects was presented in [11], where clustering techniques are used to group defects.

Detection of the surface-defects is an important part of all these methods; precise detection of the surface-defects is an important part of all these methods. Some work has been done on improving the detection of these defects: in [12], an improved set of defect residuals are found, [13] deals with a time frequency-based method and an extended threshold method, and [14] uses a wavelet packet method. In this paper, the performances of these different methods are compared. In addition, the importance of the detection precision is investigated by simulation of consequences of the different detection delays for a surface-defect. These simulations are performed assuming that, during the period of detection of the surface-defects, the defect component on the position measurements can be perfectly removed. The simulation subsequently gives the focus and radial position as response of the different detection times detection delays. The position is required to be inside some narrow bounds ($\pm 0.8\,\mu$m for focus and $\pm 0.08\,\mu$m for radial).

In Section 2, a short introduction to the CD player is given, and the consequences of the surface-defects are described as well. In Section 3, the different investigated defect detection methods are described. The simulation of the focus and radial position, depending on the defect detection times delays, are presented in Section 4. Finally, in Section 5, the conclusion is drawn.

2. THE CD PLAYER AND SURFACE-DEFECTS

2.1. The CD player

The experimental setup consists of a CD player with a three-beam single-Foucault detector principle, a PC with an I/O-card, and some hardware in order to connect the CD player with the I/O-card. Due to the limited computational power of the CPU in the PC, the sample frequency is chosen to 35 kHz. This is lower than the normal CD servo sample frequency (44 kHz). The optical pick-up in the CD player can be positioned in two directions called focus and radial, see Figure 1. These movements are controlled in the way that the focus and radial distances, e_f and e_r, are minimized.

The four-photo-detector signals are measured, denoted by $s_1[n]$, $s_2[n]$, $s_3[n]$, and $s_4[n]$, these are the elements in the vector $\mathbf{s}_m[n]$. $s_1[n]$ and $s_2[n]$ relate to the focus position and $s_3[n]$ and $s_4[n]$ relate to the radial position. The standard way of using these signals is to approximate $e_f[n] \approx s_1[n] - s_2[n]$ and $e_r[n] \approx s_3[n] - s_4[n]$, which are good approximations for small position errors, see [15].

The distances are illustrated in Figure 1. The pairwise sums of the detector signals $(s_1[n]+s_2[n])$ and $(s_3[n]+s_4[n])$ are often used as residuals for detection of surface-defects since the sums of the signal pairs depend on the total reflected laser energy. A surface-defect changes the structure of the disc surface, and thereby changes the path of the laser beam. That is, a larger part of the laser will not be reflected back on the detectors in the optical pick-up. However, these residuals are not totally independent of the pick-up position. In this paper, the signals are preprocessed in order to calculate residuals which are better decoupled from the pick-up position, see [12], these residuals are denoted α_f, and α_r for the focus and radial residuals, respectively.

2.2. Model of CD drive

A dynamical model of the CD drive is used to design a Kalman estimator which is used in the scheme extracting the decoupled residuals as well as the detection schemes. The model consists of three parts: a model of the electromagnetic system, a model of the optical detectors and a model of the surface-defects. These part models are subsequently described.

Model of the electromagnetic system

The electromagnetic system in the CD player is modeled and described in a number of publications. The focus and radial model are much alike, and are often modeled by decoupled

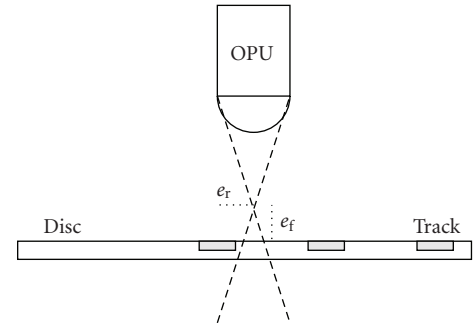

Figure 1: The focus distance, e_f, is the distance from the focus point of the laser beam to the reflection layer of the disc; the radial distance, e_r, is the distance from the center of the laser beam to the center of the track.

second-order transfer functions, see [15–18]. In a state-space format, the model is given as

$$\begin{aligned}\dot{\eta}(t) &= \begin{bmatrix}\mathbf{A}_f & \mathbf{0}\\ \mathbf{0} & \mathbf{A}_r\end{bmatrix}\cdot\eta(t) + \begin{bmatrix}\mathbf{B}_f & \mathbf{0}\\ \mathbf{0} & \mathbf{B}_r\end{bmatrix}\cdot\mathbf{u}(t),\\ \begin{bmatrix}e_f(t)\\ e_r(t)\end{bmatrix} &= \begin{bmatrix}\mathbf{C}_f & \mathbf{0}\\ \mathbf{0} & \mathbf{C}_r\end{bmatrix}\cdot\eta(t),\end{aligned} \tag{1}$$

where $\eta(t)$ is the vector of states in the model, $u_f[n]$ is the focus control signal, $u_r[n]$ is the radial control signal, both control signals are voltage applied to two linear electromagnetic actuators, $\mathbf{A}_f \in \mathcal{R}^{2\times2}$, $\mathbf{B}_f \in \mathcal{R}^{2\times1}$, $\mathbf{C}_f \in \mathcal{R}^{1\times2}$ are the state-space matrices in the focus model, and $\mathbf{A}_r \in \mathcal{R}^{2\times2}$, $\mathbf{B}_r \in \mathcal{R}^{2\times1}$, $\mathbf{C}_r \in \mathcal{R}^{1\times2}$ are the state-space matrices in the radial model. In this model, cross-couplings and a parasitic mechanical mode have been neglected since they only have minor influence on the response of the frequency range considered in this paper.

Model of the optical detectors

The optical model, mapping from physical focus and radial errors to the four-detector signals, is expressed by the vector mapping described as follows:

$$\mathbf{f}:\left(\begin{bmatrix}e_f(t)\\ e_r(t)\end{bmatrix}\right)\longrightarrow\begin{bmatrix}s_1(t)\\ s_2(t)\\ s_3(t)\\ s_4(t)\end{bmatrix}. \tag{2}$$

The mapping $\mathbf{f}(e_f(t), e_r(t))$, with a good approximation, can be separated into a product of two mappings: one mapping representing the focusing of the OPU which only depends on the focus error, the second mapping representing the placement of the OPU in the radial direction. The latter mapping only depends on the radial error. This separation into a product of two functions results in the following model:

$$f_i(e_f(t), e_r(t)) \approx h_i(e_f(t))\cdot g_i(e_r(t)), \tag{3}$$

where

$$i \in \{1, 2, 3, 4\}, \tag{4}$$

moreover,

$$g_1(e_r(t)) = g_2(e_r(t)) \tag{5}$$

since both mappings relate to the main beam. More specifically, they represent the main beam energy reflected from the surface, that is, they represent the same mapping, and the difference between D_1 and D_2 is to be found in $h_1(e_f)$ representing the Foucault principle. In [19], detailed optical models are described. In practice, it is useful to simplify this model. This can be done by approximating $h_i(e_f[n])$ and $g_i(e_r[n])$ with cubic splines, using curve fitting, see [12] in which the approximation is derived based on data.

Model of the surface-defects

Surface-defects decrease the energy received in all the detectors. This can be described by scaling the photo detector signals such that the two-focus detectors are scaled with one scale, $1 - \alpha_f(t)$, and the two-radial detectors are scaled with another one, $1 - \alpha_r(t)$. However, if these scalings were the only influence from the surface-defects on the detector signals, the surface-defect components could be removed from the detector signals by normalization of the detector signals. The surface-defect, however, also introduces a pair of defecty error components represented by a vector $\check{\mathbf{e}}(t)$, see [20, 21] . These surface-defects components are illustrated for the focus detector in Figure 2. This leads to the subsequent model of the detector signals during a surface-defect. $1 - \alpha_f[n]$ and $1 - \alpha_r[n]$, respectively, scale the focus and radial output of the optical model in which the defect error components ($\check{\mathbf{e}}[n]$) are added to the error signal ($\mathbf{e}[n]$). The vector of measured optical signals are denoted as $\mathbf{s}_m(t)$. An example of $\alpha_f(t)$, during a surface-defect, can be seen in Figure 3:

$$\mathbf{s}_m(t) = \begin{bmatrix} (1-\alpha_f(t))\cdot\mathbf{I} & \mathbf{0} \\ \mathbf{0} & (1-\alpha_r(t))\cdot\mathbf{I} \end{bmatrix} \cdot \mathrm{f}(\mathrm{e}(t) + \check{\mathbf{e}}(t)) \ . \tag{6}$$

From this model, it can be seen that the detection of the surface-defects can be based on the residuals $\boldsymbol{\alpha}_f(t)$ and $\boldsymbol{\alpha}_r(t)$ since these decrease the received energy at the detectors. These decreased detected energy levels are not the main problem since these can actually be removed by normalizing the detector signals. It is the defect component on the position measurements, denoted $\check{\mathbf{e}}(t)$, which causes the problems for the CD drive to follow the track on the disc. The controllers would try to suppress $\check{\mathbf{e}}(t)$, resulting in the CD drive being wrongly positioned. The system will, in even a few samples, diverge from the correct position into a false one. If this false position is too far away from the correct one, the tracking can be lost when the defect has been passed. In order to investigate the consequences of different surface-defect detection delays, simulations of the system, during a defect accommodated with different detection delays, are done in Section 4. In these simulations, it is assumed that after the defect is detected, it can be perfectly removed from the position measurements.

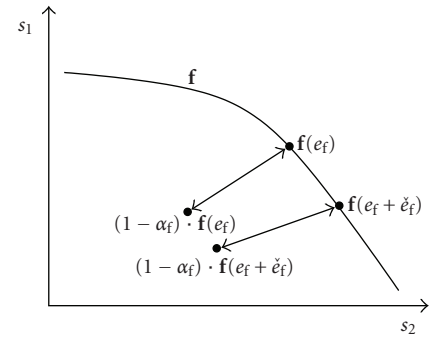

Figure 2: Illustration of how the surface-defect influence the focus measurements s_1 and s_2 for a fixed radial position $(1-\alpha_f)\cdot\mathbf{f}(e_f+\check{e}_f)$ is the measured point parameterized with α_f and $\check{e}_f$. $\mathbf{f}(e_f)$ is the point where the measurements would have been if no surface-defect were present.

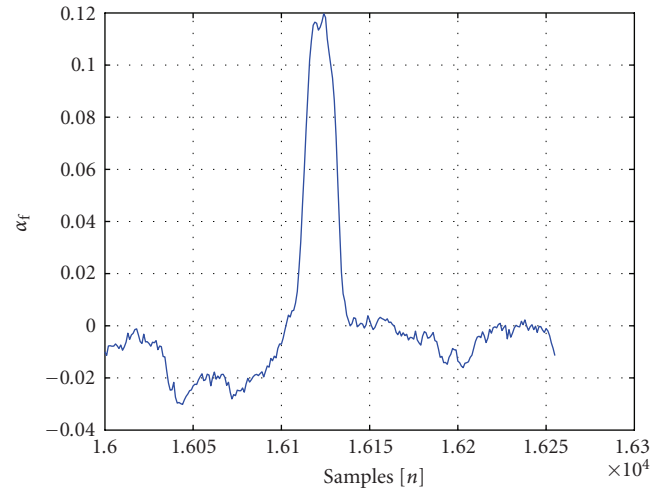

Figure 3: The focus residual α_f during a defect.

3. INVESTIGATED SURFACE-DEFECT DETECTION METHODS

First, in this section, the previously mentioned decoupled residual generation is introduced, followed by two different proposed detection schemes: an extended threshold and a wavelet packet-based detection. The first is used to investigate the time-based detection scheme and the second the joint time-frequency-based detection scheme.

3.1. Decoupled residual generation

The residual generator, which is described in [12], uses an iterative computation of the inverse of the optical mapping to generate the residual pair $\boldsymbol{\alpha}(t)$. $\alpha_f(t)$ and $\alpha_r(t)$ are fed to the defect detection which detects the surface-defects based on these residuals. With respect to the methods presented below, it is optional to use the decoupled residuals to detect the surface-defects; the normally used sum signals can be used instead for simplicity and reduced computational burden. However, the decoupled residuals have, in experiments,

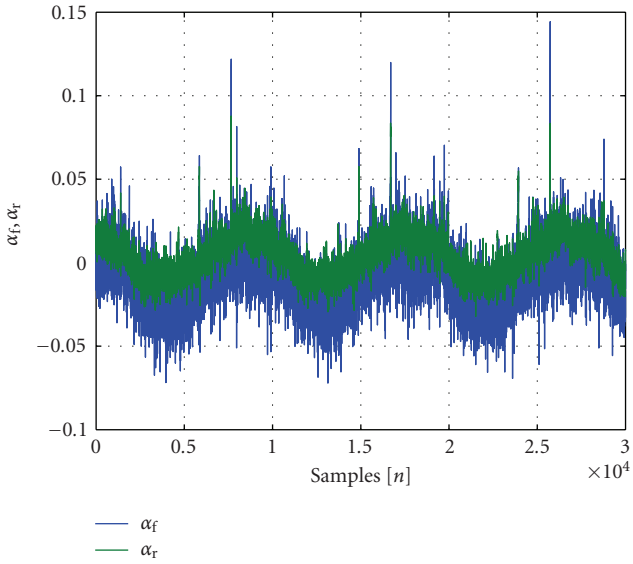

Figure 4: The two residuals $\alpha_f[n]$ and $\alpha_r[n]$ computed for a disc with a scratch and a skewness problem.

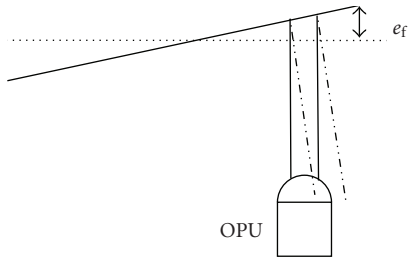

Figure 5: Illustration of the skewness of the disc. Notice that not all the reflected light do reach the OPU.

improved the detection of the defects with 1–3 samples for both the beginning and the end of the defects.

3.2. Thresholding and extended thresholding

Using thresholds for time localization of the defect has a problem in the skew discs. The skewness of the disc results in oscillating references to the focus and radial distances, which are handled by the controllers. The decoupled residuals are designed in a way such that they should be decoupled from these distances. However, in addition to these variations, the skewness also results in oscillations in the received amount of energy at the detectors. This can be seen as oscillations in the residuals $\alpha_f[n]$ and $\alpha_r[n]$. The skewness is illustrated in Figure 5 where it can be seen that a skew disc does not reflect all the light back to the OPU. A pair of residuals with a clear skewness problem is illustrated by a measured example from a disc with a scratch and a skewness problem, see Figure 4. In the following, an ad-hoc method for handling this problem is suggested. If threshold-based detection is performed on these residuals, the required threshold for detection of the defects is dependent on the defects location on the disc, and if the defect is placed at the top of the oscillation, this choice

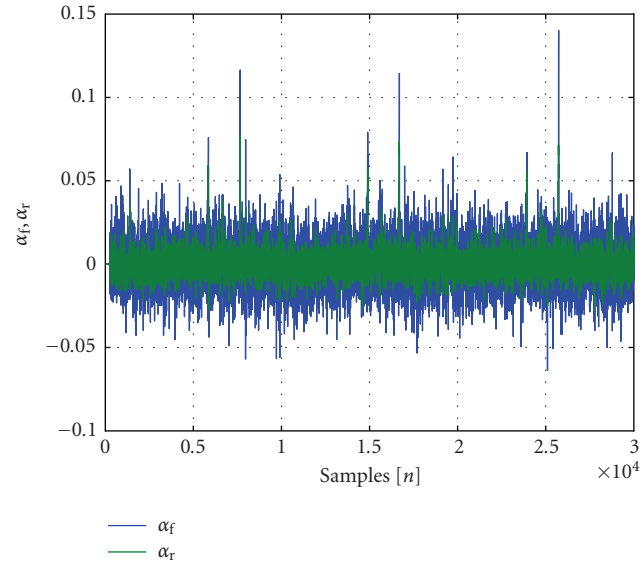

Figure 6: The skewness component is removed from the two residuals $\alpha_f[n]$ and $\alpha_r[n]$ computed for a disc with a scratch and a skewness problem.

needs to be high to ensure no false positive detections. This means a late detection of real faults. The skewness component in the signal is low-frequent, almost quasi-constant, (it is the rotational frequency of the CD). It can be removed, at sample n, by subtracting the mean of the block of samples $[n - 2^k, n - 1]$, where k is chosen in a way that the block is not too short or long. This scheme results in a high pass FIR filter, where the window length determines the crossover frequency. The window length is a power of 2 due to the usage of wavelet filters, and the specific length is found such that the longest recorded defects can be contained in one window. Using this method, the skewness components are removed from the example, see Figure 6. An alternative to this method is the use of a notch filter, which should be adapted to the given rotation frequency.

Extended threshold

To avoid the mean to change during a defect, these mean blocks need to be much longer than the defect itself. This is not an optimal solution since a long mean block requires either a large memory or a large number of computations. By inspection, it is seen that this skewness component does not change during defects. This means that one ad-hoc solution to the mean problem is to fix the mean from the sample where the defect is detected to the sample of one block length after the end of the defect. The block mean is implemented in (9) and (11).

Noises in $\alpha_f[n]$ and $\alpha_r[n]$ make it difficult to use an absolute threshold. Instead, a relative one to the variance of the nondefect residual parts can be used.

If a specific surface-defect has been met once, the time location of the next encounter is relatively well known, meaning that it can be predicted when the next encounter will be

within a short interval of samples. During this interval, a low threshold can be used. The two thresholds for beginning and end of defect detection, γ_{beg} and γ_{end}, improve the detection of the end of the defect, implemented in (8) and (10).

The mapping from the two residuals to one detection signal is proposed in [12], simply by taking the ∞ norm of the two detections. The detection decision schemes can now be described by

$$d[n] = \parallel d_{\text{f}}[n] \;\; d_{\text{r}}[n] \parallel_{\infty}, \tag{7}$$

where

$$d_{\text{f}}[n] = \begin{cases} 1 & \text{if} \dfrac{\widetilde{\alpha}_{\text{f}}[n]}{\text{var}\,(\alpha_{\text{f}})} > \gamma_{\text{beg}} \bigwedge d_{\text{f}}[n-1] = 0, \\ 1 & \text{if} \dfrac{\widetilde{\alpha}_{\text{f}}[n]}{\text{var}\,(\alpha_{\text{f}})} > \gamma_{\text{end}} \bigwedge d_{\text{f}}[n-1] = 1, \\ 0 & \text{otherwise} \end{cases} \tag{8}$$

$$\widetilde{\alpha}_{\text{f}}[n] = \alpha_{\text{f}}[n] - \text{mean}(\alpha_{\text{f}}[n-2^k,\, n-1]), \tag{9}$$

and

$$d_{\text{r}}[n] = \begin{cases} 1 & \text{if} \dfrac{\widetilde{\alpha}_{\text{r}}[n]}{\text{var}\,(\alpha_{\text{r}})} > \gamma_{\text{beg}} \bigwedge d_{\text{r}}[n-1] = 0, \\ 1 & \text{if} \dfrac{\widetilde{\alpha}_{\text{r}}[n]}{\text{var}\,(\alpha_{\text{r}})} > \gamma_{\text{end}} \bigwedge d_{\text{r}}[n-1] = 1, \\ 0 & \text{otherwise} \end{cases} \tag{10}$$

$$\widetilde{\alpha}_{\text{r}}[n] = \alpha_{\text{r}}[n] - \text{mean}(\alpha_{\text{r}}[n-2^k,\, n-1]) \tag{11}$$

The thresholds γ's are found based on data such that false detections are avoided. It should benoticed that the variance of the two residuals in the scheme are computed based on present data.

Results on the extended threshold methods

The extended and the normal threshold methods are applied to four representative defects chosen among a large number of measured defects. The thresholds are found such that false positive detections are avoided, meaning that both methods should give almost the same beginning detection of the beginning and the end of the defect.

3.3. Wavelet packet methods

It is difficult to separate the surface-defects from the disturbances in time or frequencies only. That is, it might be useful to use a wavelet packet-based detection filter, which is a joint time and frequency method. The idea is to use the wavelet packet filter bank representation to find an FIR filter, which supports the defects and can whereby be used to detect the defects. A wavelet packet transform might be used to separate the surface-defects from the disturbances, and thereby detect the surface-defects. This wavelet packet transform is done by a basis shift from the standard time basis to the best wavelet packet basis. This basis is the best wavelet packet basis given certain requirements. The wavelet package basis as well as the best basis and the joint best basis methods are shortly introduced. For more details, see [22, 23].

Wavelet packet basis

The wavelet packet transform is formed by a number of wavelet transforms. Define a signal space containing one of the residuals (α_{f} and α_{r}) as S_i. The wavelet transform separates a signal space S_i into an approximation space S_{i+1} and a detail space D_{i+1} by dividing the original basis $(\Psi_i(t - 2^i n))n \in N$ into two new orthogonal bases

$$\begin{aligned} &\left(\Psi_{i+1}(t-2^{i+1}n)\right)_{n\in N} \text{ of } S_{i+1}, \\ &\left(\Phi_{i+1}(t-2^{i+1}n)\right)_{n\in N} \text{ of } D_{i+1}, \end{aligned} \tag{12}$$

where N is a set of integers, and Ψ and Φ are, respectively, the wavelet function and its related scaling function. This decomposition is called the wavelet decomposition. The wavelet packet decomposition is formed if the approximation and details are decomposed once more such that a tree structure is formed.

The discrete wavelet decomposition can be performed by the use of two filters: h, a low-pass filter, and g, a high-pass filter. The subspaces, also called atoms, in the wavelet packet tree can be indexed by depth called level, i, and the number of subspaces, p. This means that a decomposition at the parent node (i, p) can be written as

$$\begin{aligned} s_{i+1}^{2p} &= \langle h, s_i^p \rangle, \\ s_{i+1}^{2p+1} &= \langle g, s_i^p \rangle, \end{aligned} \tag{13}$$

where s_i^p is the orignal signal, and s_{i+1}^{2p} and s_{i+1}^{2p+1} are, respectively, the approximation and details of the signal. Notice the down-sampling of the signal, which provides that the number of elements in each decomposition level does not increase. This is important in order to preserve orthogonality of the basis.

It is possible to continue this decomposition as long as the s_i^p has the length of at least 2. However, it is clear that it is possible to stop the decomposition of the tree at an earlier level and also at different levels in different parts of the tree. The final decomposition depths represent the wavelet packet basis. The question is how to find the best basis.

Best basis

A full wavelet packet tree contains a large number of possible bases. This number obviously depends on the number of levels in the tree. It can be computed recursively by $N_0 = 1$ and $N_{L+1} = 1 + N_L^2$. This clearly results in a fast decreasing number of possible bases depending on the numbers of levels in the tree, for example, for a tree with 6 levels, it is 458330, and with 7 levels $2.10 \cdot 10^{11}$.

A fast method for finding the best basis is as a consequence highly required. A fast method called the best basis search is derived in [24]. In order to measure how suitable the basis is, an information cost function is introduced. The cost function measures the cost of a given representation where the best basis has the smallest cost. Some of the commonly used information cost functions are Number of elements above a given threshold, Concentration in l^p, Entropy, and Logarithm of energy.

Having the information cost function in mind, it is possible to describe the best basis search, using the definition from [23], as follows.

(1) Compute the cost function of all elements in the wavelet packet tree.
(2) Mark all elements on the bottom level J.
(3) Let $j = J$.
(4) Let $k = 0$.
(5) Compare the cost value v_1 of element k (counting from the left) on level $j-1$ to the sum v_2 of the cost values of the elements $2k$ and $2k+1$ on level j.
    (a) If $v_1 \leq v_2$, all the marks below element k on level $j-1$ are removed, and element k is marked.
    (b) If $v_1 > v_2$, the cost value v_1 of element k is replaced with v_2.
(6) $k = k+1$. If there are more elements on level j (if $k < 2^{j-1}-1$), jump to step 5.
(7) $j = j+1$. If $j > 1$, jump to step 4.
(8) The marked basis has the lowest possible cost value. This value is found at the top element.

One should notice that this best basis is found for only one signal. In this case, this would imply that the best basis is found based on one scratch.

Joint best basis

The joint best basis is a method which takes the entire data set into account in finding the best wavelet packet basis. The joint best basis search finds the best basis given a set of signals of the same length. It could be a number of signals with encounters of the same or different scratch(es). The joint best basis algorithm computes the jointly best bases given the set of signals, information cost function, and a wavelet basis, see [23, 24]. The algorithm is as follows.

(1) Compute the full wavelet packet tree of all the signals in the signal set.
(2) Compute the tree of means by computing the mean of all signal trees at each position in the trees.
(3) Compute the tree of squares, by computing the sum of squares of all signal trees at each position in the trees.
(4) Subtract the tree of squares from the tree of means to obtain the tree of variances.
(5) Find the best basis of the tree of variance by using the best basis algorithm given an information cost function and wavelets.

A joint best basis is found in the sequel for the matrices in which the column vectors are different residuals containing defects, the matrix of focus residuals are denoted $\mathbf{F}_f$ and for the radial residuals $\mathbf{F}_r$, where some different wavelets and information cost functions were tried. The Daubechies 1–6 filters, see [22], were tried, since their filter taps look like a surface-defect, together with the l^2 and Shannon information cost functions, see [22], all the combinations of these bases and cost functions were tried with poor results.

The problem in using the joint best basis algorithm directly is the choice of information cost function and the best basis search. When used to defect detection, the scope is to find a band-pass filter, which separates the surface-defect from the background noises in the residuals. In other words, the wavelet packet atom, in which the defect is separated from the disturbances, uses the wavelet packet analysis to analyze the data in order to design an FIR filter, which is given.

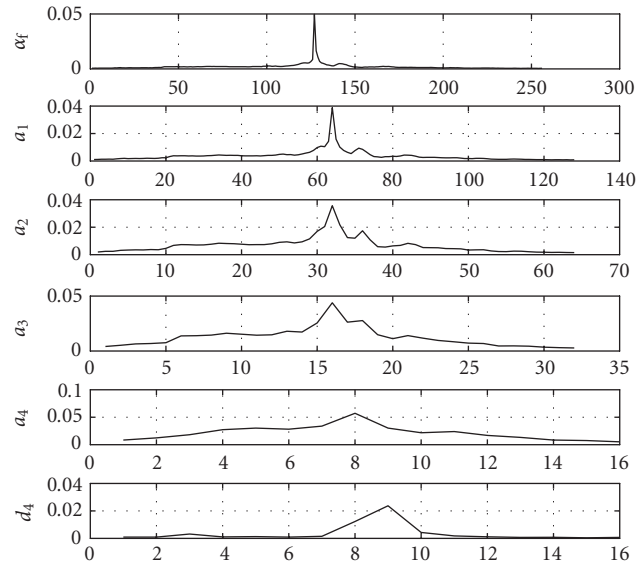

Figure 7: The part of the tree of variances of $\alpha_f[n]$, as defined in the scheme. The figure starts with the original variance signal. The second plot is *h*, the third is *hh*, the fourth is *hhh*, the fifth is *hhhh*, and the last one is *hhhg*.

Instead of using a cost function, a heuristic-based method is used. The method takes its starting point in the tree of variances used in the joint best basis algorithm. The used method consists of the following steps.

(1) Compute the tree of variances, use steps 1–4 in the joint best basis search.
(2) Search down the levels in the tree to find a level where the approximations and details both contain energy.
(3) Use the corresponding filter to this detail atom for the detection of surface-defects.

The core idea in this method is to find a frequency interval which does not contain the lowest frequencies and still contains a relative large part of energy of the defect. The related filter is subsequently used for the defect detection.

Results on wavelet packet-based scheme

This method is subsequently used on $\alpha_f[n]$ and $\alpha_r[n]$. The Haar wavelet, see [22], is used for both signals since it is well suited for detection changes in the signal, and it is short in terms of filter elements. The method is first used to analyze the $\alpha_f[n]$. By using the heuristic method, the interesting part of the tree of variances can be seen in Figure 7. The figure starts with the original variance signal. The remaining figure parts are located by denoting a low-pass filtering with *h* and high-pass filtering with *g*, meaning that two low-pass filterings followed by one high-pass are denoted *hhg*. The second

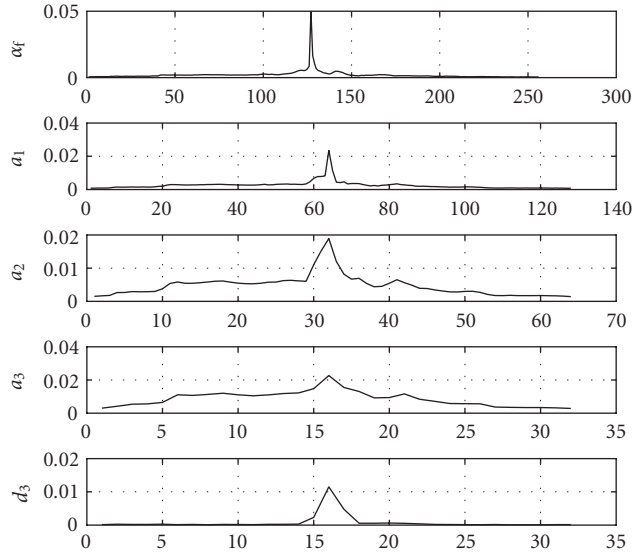

FIGURE 8: The part of the tree of variances of $\alpha_r[n]$, as defined in the scheme. The figure starts with the original signal. The second plot is h, the third is hh, the fourth is hhh, and the last one is hhg.

plot is h, the third is hh, the fourth is hhh, the fifth is $hhhh$, and the last one is $hhhg$. Notice the large change from hhh to $hhhh$, which results in a significant signal in $hhhg$. The details with low energy have been left out in the plot. This signal is useful for defect detection since it has relatively large signal parts and does not contain the near zero frequencies where disturbances are dominating. This means that a useful filter for defect detection in $\alpha_f[n]$ is found. It is three Haar low-pass filters followed by one Haar high-pass filter. The wavelet filters are in the defect detection used as normal FIR filters where the wavelet filter coefficients are used as the coefficients in an FIR filter. That is,

$$y[n] = a_1 \cdot x[n] + a_2 \cdot x[n+1] + \cdots + a_N \cdot x[n+N-1], \tag{14}$$

where N is the length of the filter. This is in contrast to the normal usage of the wavelet packet filters where the output $y[n]$ depends on both causal and noncausal inputs $x[n]$, and is processed block by block. Instead, a filtered signal is computed at each sample. The wavelet packet analysis is thereby used to analyze the data. Based on this wavelet packet analysis, an FIR filter is designed using the Haar wavelet.

The same method is applied to $\alpha_r[n]$, using the same wavelet, the Haar wavelet. The interesting part of the tree of variance can be seen in Figure 8. The figure starts with the original signal. The remainder of the figure is in the focus case, however, the analysis stops a level earlier in the radial case. Notice the large change from hh to hhh, which results in a significant signal in hhg. The same conclusions can be drawn for the radial filters as for the focus filter. It should be noted that the detection scheme is depending on the wavelet basis used for the detection.

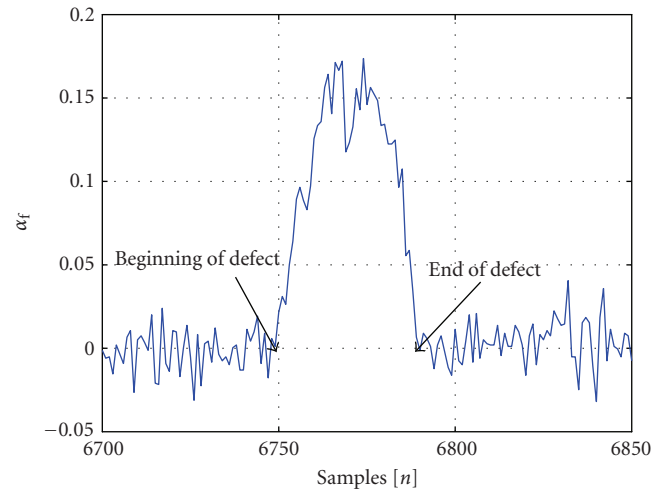

FIGURE 9: A zoom on the α_f during scratch no. 1.

3.4. Verification and comparison of the method

A zoom on a defect from the test set is shown in Figure 10. From this figure, it is seen that the filtered signal starts with negative values and subsequently takes positive values. The first part is a response to the beginning of the defect and the second one is the response to the last part of the signal. This means that the detection of the beginning of the defect can be performed by the absolute filtered signal's first crossing of a threshold. The end is detected by the fourth crossing of this threshold where the absolute filtered signal is lower than the threshold. This approach is illustrated on α_f during defect #1 in Figure 10. The nonmanipulated α_f in this case is shown in Figure 9.

A threshold is subsequently used on these signals to locate the surface-defects in time, see Figure 10, or in other words to detect the defects. The threshold is found as the smallest one, which does not result in any false positive detection.

This wavelet packet-based FIR filter design relates a matched filter in which the filter coefficients are equal to the signal it should detect. Using this filter type, a filter will be optimal to detect the defect its design is based on, but it might not detect other defects. Since the proposed wavelet packet-based scheme is designed to deal with more than one defect, it is better suited to deal with the problem of detecting surface-defects on CDs.

3.5. Summary of the proposed detection schemes

The results of the proposed detection schemes are applied to 4 different defects, and can be seen in Table 1. A detection delay at the beginning of a defect means the number of samples; the detection of the beginning is delayed compared with the actual beginning of the defect. A detection delay at the end of defect means the number of samples; the end is detected earlier than the actual end of the defect.

Both the extended threshold method and the wavelet packet-based method detect the defect well and better than a

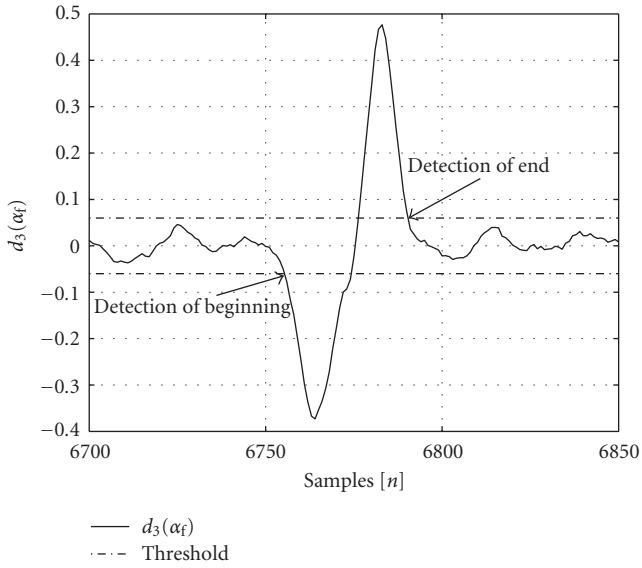

FIGURE 10: A zoom on scratch (defect) no. 1 in $\alpha_f[n]$ filtered with three Haar low-pass filters followed by one high-pass filter.

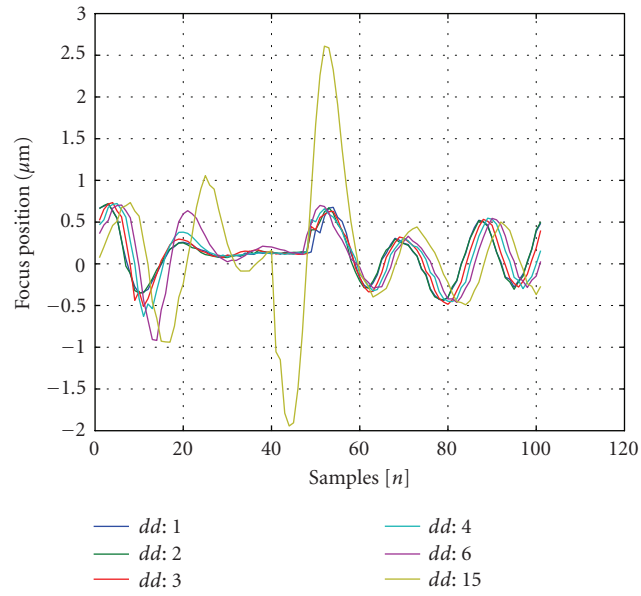

FIGURE 11: Simulation of the effect of detection delays on the closed loop focus position.

TABLE 1: The detection of the four scratch examples, where the wavelet packet-based method is compared with normally used standard threshold method. In the table, the detection delays of these two methods for the four examples are shown.

Defect	α_f, α_r	Normal (beg.)	Normal (end)	Ext (beg.)	Ext (end)	WP (beg.)	WP (end)
No. 1	α_f	13	5	3	3	6	4
	α_r	7	7	4	0	5	4
No. 2	α_f	2	4	2	2	1	1
	α_r	5	7	3	5	2	4
No. 3	α_f	2	3	1	0	2	1
	α_r	3	5	2	3	2	3
No. 4	α_f	21	5	2	1	6	3
	α_r	22	6	21	5	21	3

traditional threshold. It is also seen that the extended threshold detection scheme detects the defects approximately 1 sample faster except for defect number three were the wavelet packet-based scheme detects the defect one sample earlier. It should also be noted that the wavelets filters used clearly depends on the actually meant defects, the detection filters should give good support of the defect in order, for the filter, to detect the defect. This fact leads to the usage of the joint best basis for the wavelet basis search, since the filter consequently would be trained to detect a number of defects. The used wavelet filter will consequently influence the detection, meaning that other wavelet filters might improve the detection. This detection problem relates to the work of classifying surface-defects, where [11] presents an extensive study on defect classification, using clustering techniques.

All these results are relatively transparent to usage at other optical disc drives such as DVD, Blue-ray, and so forth. The only problem is to adjust the models and parameter to the given drive. It could also be relevant to introduce other time-frequency-based detection filters.

4. SIMULATION OF THE CONSEQUENCE OF THE DEFECT DETECTION PERFORMANCE

A simulation model developed in [21] is used to simulate the effect of the previously mentioned detection delays on the close loop system (for both the focus and the radial position). Surface-defect no. 1, from the experiments with detections, is used in these simulations. In the simulations, it is assumed that the defect component in the position measurement can be perfectly removed when the defect is detected. The simulations are performed for a detection delay of 1, 2, 3, 4, 6, and 15 samples delay at the beginning and the end of the defect. The focus position simulations are plotted in Figure 11, and the radial position simulations are plotted in Figure 12. For both plots, it can be seen that positions are increasingly influenced by the defects as the detection delay increases, the 15 samples delay will lead both focus and radial, and the 6 samples delay for the focus case will be outside the normal operation range (.8 μm for focus and .08 μm for radial), resulting in a lost focus and lost tracking. It shall be noticed that for more severe scratches, the focus and tracking can be lost at much lower-detection delays at only a few samples, meaning that an improvement of a detection method of only a sample compared to other detection schemes can eventually turn out to make it possible to play a disc with a certain scratch.

5. CONCLUSION

Online detection of surface-defects on optical discs is of high importance for the accommodation schemes handling these defects. These surface-defects introduce faulty components

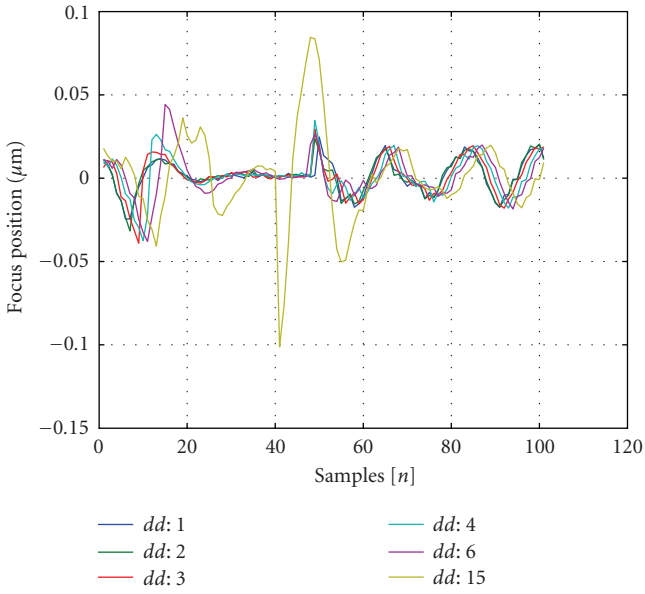

FIGURE 12: Simulation of the effect of detection delays on the closed loop radial position.

to the position measurements of focus and radial tracking positions. The respective controllers will accordingly try to suppress these defecty components, resulting in a wrong positioning of the optical disc drive. In this paper, three different schemes for detecting these surface-defects are introduced and compared. Two of these methods, an extended threshold scheme and a wavelet packet-based scheme, improve the detection compared with a standard threshold scheme. The extended threshold scheme detects the four tested defects with a maximal detection delay of 3 samples, while the wavelet packet-based scheme has a maximal detection delay of 6 samples. Simulations of focus and radial positions in the presence of surface-defects are performed in order to inspect the importance and consequences of the size of the detection delay. From the simulation, it can be seen that focus and radial positions increase significantly due to the defect as the detection delay increases.

ACKNOWLEDGMENTS

The authors acknowledge the Danish Technical Research Council for support to the research program WAVES (Wavelets in Audio Visual Electronic Systems), Grant no. 56-00-0143. The authors acknowledge the Danish Ministry of Science, Technology, and Innovation for support to the research program CMBC (Center for Model-Based Control), Grant no. 2002-603/4001-93.

REFERENCES

[1] M. Steinbuch, G. Schoostra, and O. Bosgra, "Robust control of a compact disc player," in *Proceedings of the 31st IEEE Conference on Decision and Control (CDC '92)*, vol. 3, pp. 2596–2600, Tucson, Ariz, USA, December 1992.

[2] W. Draijer, M. Steinbuch, and O. Bosgra, "Adaptive control of the radial servo system of a compact disc player," *Automatica*, vol. 28, no. 3, pp. 455–462, 1992.

[3] H. G. M. Dötsch, H. T. Smakman, P. M. J. van den Hof, and J. Steinbuch, "Adaptive repetitive control of a compact disc mechanism," in *Proceedings of the 34th IEEE Conference on Decision and Control (CDC '95)*, vol. 2, pp. 1720–1725, New Orleans, La, USA, December 1995.

[4] G. Hearns and M. Grimble, "Limits of performance of an optical disk drive controller," in *Proceedings of the American Control Conference (ACC '99)*, vol. 5, pp. 3625–3629, San Diego, Calif, USA, June 1999.

[5] L. Yao, A.-M. Wang, and Y.-F. Cheng, "Track seeking hybrid fuzzy controller for the compact disc player," in *Proceedings of the 10th IEEE International Conference on Fuzzy Systems (FUZZ '02)*, vol. 3, pp. 1589–1593, Melbourne, Australia, December 2002.

[6] M. Steinbuch, "Repetitive control for systems with uncertain period-time," *Automatica*, vol. 38, no. 12, pp. 2103–2109, 2002.

[7] Philips, "Product specification: digital servo processor DSIC2," Tech. Rep. TDA1301T, Philips Semiconductors, Eindhoven, The Netherlands, March 1994.

[8] P. Andersen, T. Pedersen, J. Stoustrup, and E. Vidal, "Method for improved reading of digital data disc," International patent, no. WO 02/05271 A1, 2001.

[9] E. Vidal Sánchez, *Robust and fault tolerant control of CD-players*, Ph.D. dissertation, Department of Control Engineering, Aalborg University, Aalborg, Denmark, 2003.

[10] P. F. Odgaard, J. Stoustrup, P. Andersen, M. V. Wickerhauser, and H. F. Mikkelsen, "Feature-based handling of surface faults in compact disc players," *Control Engineering Practice*, vol. 14, no. 12, pp. 1495–1509, 2006.

[11] J. van Helvoirt, G. Leenknegt, M. Steinbuch, and H. Goossens, "Disc defect classification for optical disc drives," *IEEE Transactions on Consumer Electronics*, vol. 51, no. 3, pp. 856–863, 2005.

[12] P. F. Odgaard, J. Stoustrup, P. Andersen, and H. F. Mikkelsen, "Detection of surface defects and servo signal restoration for a compact disc player," *IEEE Transactions on Control Systems Technology*, vol. 14, no. 2, pp. 189–203, 2006.

[13] P. F. Odgaard and M. V. Wickerhauser, "Time localisation of surface defects on optical discs," in *Proceedings of IEEE International Conference on Control Applications (CCA '04)*, vol. 1, pp. 111–116, Taipei, Taiwan, September 2004.

[14] P. F. Odgaard, J. Stoustrup, P. Andersen, and M. Wickerhauser, "Wavelet packet based detection of surface faults on compact discs—a joint best basis approach," in *Proceedings of 6th IFAC Synposium on Fault Detection Supervision and Safety of Technical Processes (SAFEPROCESS '06)*, pp. 1165–1170, Beijing, China, August 2006.

[15] W. Bouwhuis, J. Braat, A. Huijser, J. Pasman, G. van Rosmalen, and K. S. Immink, *Principles of Optical Disc Systems*, Adam Hilger, Bristol, UK, 1985.

[16] S. G. Stan, *The CD-ROM Drive: A Brief System Description*, Kluwer Academic Publishers, Norwell, Mass, USA, 1998.

[17] E. Vidal, J. Stoustrup, P. Andersen, T. Pedersen, and H. F. Mikkelsen, "Open and closed loop parametric system identification in compact disk players," in *Proceedings of the American Control Conference (ACC '01)*, vol. 4, pp. 3294–3298, Arlington, Va, USA, June 2001.

[18] E. Vidal, K. G. Hansen, R. S. Andersen, et al., "Linear quadratic controller with fault detection in compact disk players," in *Proceedings of the IEEE International Conference on Control*

Applications (CCA '01), pp. 77–81, Mexico City, Mexico, September 2001.

[19] P. F. Odgaard, J. Stoustrup, P. Andersen, and H. F. Mikkelsen, "Modelling of the optical detector system in a compact disc player servo system," in *Proceedings of the American Control Conference (ACC '03)*, vol. 4, pp. 3101–3106, Denver, Colo, USA, June 2003.

[20] P. F. Odgaard, J. Stoustrup, P. Andersen, and H. F. Mikkelsen, "Estimating focus and radial distances, and fault residuals from CD player sensor signals by use of a Kalman estimator," in *Proceedings of the 42nd IEEE Conference on Decision and Control (CDC '03)*, vol. 2, pp. 1962–1967, Maui, Hawaii, USA, December 2003.

[21] P. F. Odgaard, J. Stoustrup, P. Andersen, M. Wickerhauser, and H. F. Mikkelsen, "A simulation model of focus and radial servos in compact disc players with disc surface defects," in *Proceedings of the IEEE International Conference on Control Applications (CCA '04)*, vol. 1, pp. 105–110, Taipei, Taiwan, September 2004.

[22] S. Mallat, *A Wavelet Tour of Signal Processing*, Academic Press, New York, NY, USA, 2nd edition, 1999.

[23] M. Wickerhauser, *Adapted Wavelet Analysis from Theory to Software*, A K Peters, Natick, Mass, USA, 1st edition, 1994.

[24] R. R. Coifman and M. Wickerhauser, "Entropy-based algorithms for best basis selection," *IEEE Transactions on Information Theory*, vol. 38, no. 2, pp. 713–718, 1992.